Tellus (2006), 58A, 508–519
Printed in Singapore. All rights reserved

TELLUS

Atmospheric angular momentum balance for the southern hemisphere during the polar vortex break-up of September 2002

By DIETER PETERS* and CHRISTOPH ZÜLICKE, *Leibniz-Institut für Atmosphärenphysik an der Universität Rostock e.V., Schlossstraße 6, D-18225 Ostseebad Kühlungsborn, Mecklenburg, Germany*

(Manuscript received 1 April 2005; in final form 3 February 2006)

ABSTRACT

The evolution of the axial component of the atmospheric angular momentum vector (AAM) is investigated for September 2002, using ECMWF analyses. The components of the conservation equation of AAM for southern polar cap volume are calculated in order to examine the importance of their contributions to the AAM tendency during the unexpected break-up of the southern polar vortex in the last week of September.

The AAM tendency for the mean polar cap (90°–65° S) oscillates with a period of 5 d until the break-up of the polar vortex, after that it is negative for about 9 d. The polar friction torque induced by katabatic winds is weakly positive and nearly constant. For this mean polar cap, the mountain torque at the surface is mainly positive and larger than the friction torque. The strong changes of the mountain torque are caused by shifts of surface pressure patterns induced by a Rossby wave train touching the orography of Antarctica. The fluxes of AAM are northwards and reduce the AAM of the polar cap volume. The changes of AAM fluxes are mainly determined by the evolution of momentum fluxes due to transient Rossby waves in the upper troposphere and lower stratosphere. The vortex break-up is associated with a strong decrease of the amount of mountain torque and an increase in the convergence of relative AAM fluxes.

1. Introduction

For the first time a mid-winter stratospheric sudden major warming was observed in the southern hemisphere in September 2002 (e.g. Baldwin et al., 2003; Simmons et al., 2003). The World Meteorological Organisation criterion for a major warming is fulfilled on 26 September and indicated by a reversal of the meridional temperature gradient between 60° S and the South Pole (Krueger et al., 2005). The definition of a major warming includes also a breakdown of the polar vortex by the reversal of the zonal mean zonal wind from westerlies into easterlies poleward of 60° S, at least down to 10 hPa.

In Fig. 1, the zonal mean zonal wind is plotted at 60° S latitude for September 2002. In the upper stratosphere, the mean zonal wind oscillates and shows a reversal from westerlies to easterlies down to 10 hPa, which indicates the sudden major warming, during late September. After few days, the mean westerlies have been re-established for duration of 3 wk (not shown). The final warming with a reversal of the mean zonal wind into easterlies occurred earlier than in 2001, namely during the end of October 2002 (Baldwin et al., 2003).

Note, further information about the dynamics of the austral major warming event in September 2002 is given in a *Journal of Atmospheric Sciences Special Issue* (March 2005).

In this study we use ECMWF analyses to examine the balance of the axial component of the atmospheric relative angular momentum vector (the 'atmospheric angular momentum' or AAM, for brevity), and evolution of the components of the AAM conservation equation, in the Southern Hemisphere during September 2002. Large changes in AAM are expected during a major warming event but this has yet to be quantified.

The motivation of this study has two starting points. First, katabatic winds caused by denser air masses, which are slipping downhill, are a dominant feature in the Antarctic boundary layer in winter (Schwerdtfeger, 1984). Egger (1992) studied the atmospheric dynamics over Antarctica and showed that the generation of AAM by katabatic winds (become easterlies at about the coast line of Antarctica due to the Coriolis force) is balanced by momentum flux out of Antarctic polar cap volume through Rossby waves. These Rossby waves are modifying their phase tilt with the latitude in relation to the latitudinal slope of the Antarctic topography. Further, Peters and Egger (1993) showed with GCM simulations that the mountain torque induced by these Rossby

*Corresponding author.
e-mail: peters@iap-kborn.de
DOI: 10.1111/j.1600-0870.2006.00187.x

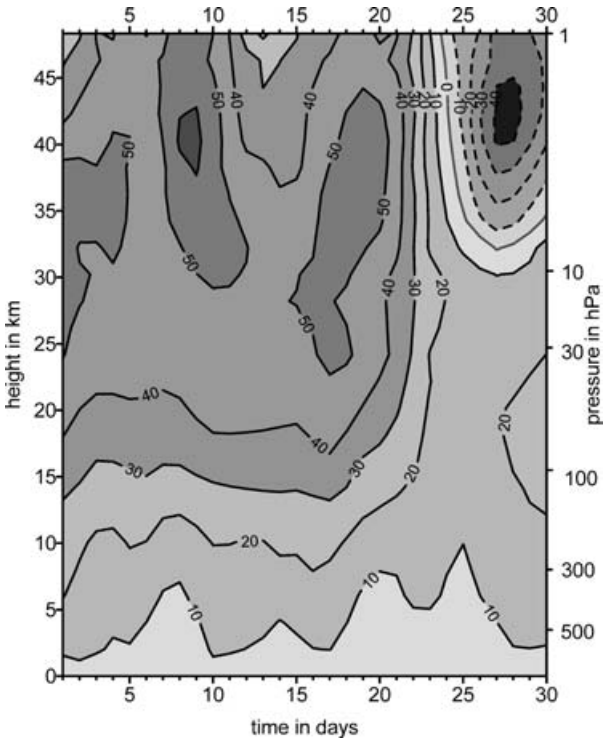

Fig. 1. Zonally averaged zonal wind in m s^{-1} at 60° S for ECMWF analyses. Dashed lines indicate easterlies.

waves also act as an important source of AAM. Both sources of AAM at southern polar latitudes are mainly balanced by AAM flux convergences of Rossby waves due to strong northward momentum fluxes at about the 300-hPa layers over about coastline of Antarctica. For a time-mean flow the tendency of zonal mean AAM vanishes, but during the evolution of the flow strong AAM imbalances of sources and sinks can cause strong tendencies of zonal mean AAM. What the balance of the components of AAM is during stratospheric sudden warming (Scherhag, 1952) is an open question, and this is one of the foci of this study.

The second starting point for this study is the general accepted theory of stratospheric sudden warming following the ideas outlined in Matsuno (1971). In Matsuno's theory, strong transient tropospheric Rossby waves propagate upwards and cause local Eliassen-Palm-flux (EP-flux) convergences in the upper stratosphere, the zonal mean zonal wind is decelerated and the air is warmed adiabatically, due to the induced descending residual circulation of the upper polar stratosphere. The resulting change in the mean state will change the Rossby wave propagation, which cause further changes in the mean state. What follows, is a sudden decelerated zonal mean zonal wind and a sudden warming in the upper polar stratosphere.

However, little is known about the forcing of strong transient tropospheric Rossby waves, which generate the warming event, and, how this forcing relates to the sudden decelerated zonal mean zonal wind. In particular, little attention has been paid to the tropospheric generation of AAM through these transient Rossby waves during warming events.

It is known that assimilation errors of observed quantities could occur in the analyses (Rosen et al., 1987), but calculations of the atmospheric AAM based on analyses, forecasts and reanalyses are very useful for further investigations and partially serve as products of weather centres. Such data sets have been used by Weickmann et al. (2000) (NCAR-analyses) and Egger and Hoinka (2002) (ECMWF-reanalyses) in order to calculate the covariance function of the components of AAM tendency. They found that for the intraseasonal time scale the global mountain torque primarily generates AAM. The global friction torque has a decorrelation time of 6 d, which means it is linked with teleconnection patterns and zonal index variations (Weickmann, 2003). In boreal winters the anomalies of the global mountain torque are generated by synoptic weather systems, which distribute their energy over the orography of Asia and North America (Iskenderian and Salstein, 1998). Latitude-band averages of mountain torque and friction torque show large differences in the balance of these two quantities as a function of latitude and time, which are caused by meridional transports of AAM by the large-scale atmospheric circulation (Newton, 1971).

For a southern hemispheric polar cap volume, defined by a vertical and longitudinal integral and an additional integral from the South Pole to any fixed latitude (virtual wall), the integration volume is independent of the Earth's rotation. The AAM balance of such a polar cap is determined by mountain torque and friction torque at the surface and by meridional AAM fluxes through a apparent latitudinal wall (e.g. Peixoto and Oort, 1992).

In austral winter strong katabatic winds generate easterlies near the coast line (Schwerdtfeger, 1984). These easterlies cause a friction torque, which is a source of AAM, similar to the trade wind in the subtropics. However, the west winds in mid-latitudes cause a sink of AAM in both hemispheres. The mountain torque for a polar cap region (e.g. 90°–65° S) also generates AAM like the friction torque (Madden and Speth, 1995), the AAM balance has to be closed by meridional transports of AAM out of the polar cap, if we assume that in the climate mean the AAM tendency is zero. In a more general AAM polar cap balance we could figure out explicitly over the evolution of imbalance, which sources or sinks (namely mountain torque, friction torque and convergence of AAM fluxes and their relation to each other) of AAM are responsible for the expected strong decrease of polar AAM during that major warming event of September 2002. That means we examine the sources or sinks of AAM, which are important for the deceleration of the zonal mean zonal wind and for the warming of the air during that major warming event.

The layout of the paper is as follows. In Section 2, the method used for AAM calculation is presented. Results are given in Section 3. We are starting with global and hemispheric AAM calculations of September 2002, then showing the extra-tropical southern hemispheric AAM balance of polar cap torques, but focusing on the polar cap AAM balance over Antarctica. The

discussion is given in Section 4, and final the conclusions in Section 5.

2. Methods of AAM calculation and data

2.1. AAM balance equation for a southern hemispheric polar cap

With the action of forces the following theorem holds for the conservation of AAM (e.g. Peixoto and Oort, 1992; Salby, 1996):

$$\frac{d}{dt}((u + \Omega a \cos\varphi) a \cos\varphi) = -a \cos\varphi \left(\frac{1}{\rho a \cos\varphi} \frac{\partial p}{\partial \lambda} + R_\lambda \right), \tag{1}$$

where $\frac{d}{dt}$ is the total derivative. (λ, φ, r) represent the spherical coordinates, Ω is the angular velocity (constant) of the Earth, r was set equal to a, the Earth's radius; $u = a \cos\varphi \frac{d\lambda}{dt}$ is the zonal velocity, p pressure, ρ density and R_λ represents the friction force in longitudinal direction. Equation (1) means that the AAM of a unit air-mass volume can only be changed through the pressure gradient force or the friction force. The absolute AAM can be rewritten as:

$$M = M_r + M_\Omega, \tag{2}$$

where

$$M_r = ua \cos\varphi \tag{3}$$

defines the relative AAM, and

$$M_\Omega = \Omega a^2 \cos^2\varphi, \tag{4}$$

the Ω-(planetary)AAM of air per unit mass. For the description of angular momentum transport in the atmosphere it is useful to integrate M over polar caps of the atmosphere, where a polar cap is bounded by the Earth's surface, the upper boundary of the atmosphere and a specified latitude. After some transformations of (1) with the continuity equation and integrating over the volume V of a southern hemispheric polar cap follows:

$$\begin{aligned} \int_{pc} \frac{\partial}{\partial t}(M\rho) dV &= -\int_{pc} \nabla \cdot (M \rho \underline{u}) dV \\ &\quad - \int_{pc} \frac{\partial p}{\partial \lambda} dV - \int_{pc} \rho a \cos\varphi R_\lambda dV, \end{aligned} \tag{5}$$

where u is the velocity vector.

After further manipulation (see, Peixoto and Oort, 1992) eq. (5) can be rewritten as

$$\begin{aligned} \frac{\partial}{\partial t} \langle [\{M\rho\}] \rangle^{\varphi_{pc}} &= -[\{M\rho v\}]|^{\varphi_{pc}} \\ &\quad + \left\langle \left[\frac{\partial p_s}{\partial \lambda} z_0 \right] \right\rangle^{\varphi_{pc}} + \langle [\tau_s a \cos\varphi] \rangle^{\varphi_{pc}} \end{aligned} \tag{6}$$

where

$$\{M\rho\} := \int_{z_0}^{\infty} M\rho dz = -\frac{1}{g} \int_{p_s}^{0} M dp = \frac{1}{g} \int_0^1 M \frac{\partial p}{\partial \eta} d\eta, \tag{7}$$

$$[M\rho] := a \cos\varphi \int_0^{2\pi} M\rho d\lambda, \tag{8}$$

$$\langle M\rho \rangle^{\varphi_{pc}} := a \int_{-\pi/2}^{\varphi_{pc}} M\rho d\varphi, \tag{9}$$

where φ_{PC} is a specified latitude (and integrals are over all altitudes, all longitudes and a specified latitudinal region (90° S $-$ φ_{PC})), v is the meridional velocity, z_0 orography, g the Earth's gravity and τ_S is the longitudinal shear stress at the surface, and η in (7) is the hybrid coordinate used in the standard ECMWF analysis.

Equation (6) represents the basic equation of this investigation. The tendency of AAM of an air volume integrated over the polar cap is equal to the sum of the polar cap convergence of AAM fluxes (which is equal to the integral over the latitudinal wall for the AAM fluxes perpendicular to the wall, Gauss theorem), the surface integral of mountain torque and that of friction torque. That means, that AAM polar cap balance changes if AAM exchanges across the bounding latitude φ_{PC} or if angular momentum exchanges between the atmosphere and the solid earth or oceans by outer forces.

2.2. Data and AAM calculation

For the evaluation of eq. (6), the daily ECMWF analyses of September 2002 at 00 UT have been obtained from the MARS (Meteorological Archival and Retrieval System) archive of ECMWF. We used standard ECMWF analyses and forecasts data (see Section 4) based on triangular 511-resolution (T511) in spectral space and 60 vertical hybrid levels. The equivalent longitude–latitude grid point resolution is 0.351 degree and the last full level before $p = 0$ is 0.1 hPa (about 66 km height). The chosen resolution was 3° longitude by 5° latitude. For the calculation of AAM and AAM fluxes, the horizontal wind at all 60 η layers was used. Further, surface pressure p_s, orography z_0, the zonal and meridional wind at a height of 10 m (u10, v10), and roughness length r_0 were also extracted from that archive. For the integral calculations of eqs. (7)–(9), the simple trapezoid rule was used and the respective derivatives were resolved by finite differences (for instance the $\frac{\partial p}{\partial \eta}$ of eq. (7)).

With eq. (6) there exist two possibilities to calculate the AAM tendency of the polar cap, explicitly with the formula on the left-hand side and as a sum of terms. The difference gives a check on the accuracy of the calculations (see below).

For ECMWF analyses, the surface stress in the lower most model layer was not available in the respective MARS data sets. Therefore, we estimate the surface stress using winds (u10, v10)

at 10 m height and the following bulk formula:

$$\tau_s = \rho_s C_D \sqrt{\left(u10^2 + v10^2\right)} * u10, \tag{10}$$

with

$$C_D = \frac{\kappa^2}{\ln^2\left(\frac{10m}{r_0} + 1\right)}, \tag{11}$$

where κ is the von Karman constant and $\rho_S = 1.225$ kg/m^{-3}. For all regions with a roughness length of $r_0 > 0.03$ m, r_0 was reset to $r_0 = 0.03$ m as the used analysed surface winds at 10 m height have been calculated under this specific assumption. This is a simplification of the parametrization operationally used for ECMWF analyses and forecasts, described in details in chapter 3 of White (2003).

Note, the gravity wave drag due to the unresolved orography was introduced in the analyses, but for this data set the induced torques were not available for post-processing. The amount of gravity wave drag torque is very small in comparison to mountain and friction torques (compare Figs. 12a and c). As we will demonstrate below this torque has no significant role for the AAM balance of a polar cap up to 60° S.

3. Results

For September 2002, the global and hemispheric monthly mean values of relative and Ω-AAM are presented in Table 1. It confirms that the global Ω-AAM is hundred times larger than the relative AAM. Consequently, the absolute AAM is dominated by Ω-AAM. The mean values are in good agreement with those of Madden and Speth (1995) estimated for September 1987, but their vertical integration was bound by 10 hPa: The Ω-AAM from Table 1 is slightly larger ($+0.4 \times 10^{26}$ kg m^2 s^{-1}) and the relative AAM slightly smaller (-0.2×10^{26} kg m^2 s^{-1}). In September 2002 the Ω-AAM of both hemispheres are similar. The relative AAM of the Southern Hemisphere is about six times larger than that of the Northern Hemisphere with a larger standard deviation of the northern hemispheric values. Also the maximum of relative AAM of the Northern Hemisphere (0.28×10^{26} kg m^2 s^{-1}) is distinctly smaller than the southern hemispheric minimum (1.02×10^{26} kg m^2 s^{-1}).

Table 1. Statistics of atmospheric angular momentum [10^{26} kg m^2 s^{-1}] for mean September 2002

	AVE M_Ω	AVE M_r	STD M_r	MIN M_r	MAX M_r
Global	101.8	1.26	0.041	1.17	1.31
NH	50.5	0.17	0.079	0.05	0.28
SH	51.3	1.09	0.057	1.02	1.19

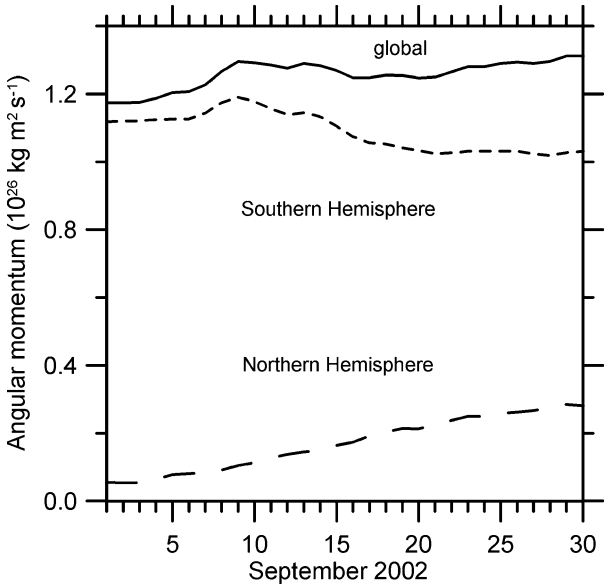

Fig. 2. Evolution of relative atmospheric angular momentum (10^{26} kg m^2 s^{-1}) for Southern Hemisphere (short dashed line), for Northern Hemisphere (long dashed line) and for both hemispheres (full line) in September 2002.

3.1. Evolution of AAM

The evolution of the axial component of the relative atmospheric angular momentum of both hemispheres in September 2002 is shown in Fig. 2. The southern hemispheric relative AAM is larger than the northern hemispheric relative AAM by a factor of about 6 as mentioned above. The northern hemispheric relative AAM increases throughout September. The southern hemispheric relative AAM has a maximum at about day 9 and decreases until day 20. Thereafter, the values are nearly constant till the end of the month. Generally, the global relative AAM shows an increase from the beginning to the end of September 2002 which is in agreement with the annual cycle found by Madden and Speth (1995). After Madden and Speth (1995), the global relative AAM undergoes an annual cycle of low values in summer and high values in winter. The global Ω-AAM has no explicit annual cycle but a wide-ranging spectrum of fluctuations depending on density variations.

The evolution of hemispheric relative AAM in Fig. 2 can be examined by means of a Hovmöller diagram of relative AAM. Figure 3 shows the evolution of vertically and zonally integrated AAM with a normalization factor to reproduce units of AAM per radian. For Northern Hemisphere, we see that relatively small positive values of Fig. 2 result from smaller values in mid-latitudes in comparison to the Southern Hemisphere. The subtropical and tropical values are negative due to the trade winds (easterlies) and reduce the hemispheric integral. The northern hemispheric AAM increases with time, which is caused by a broader west-wind band. The positive mid-latitudes

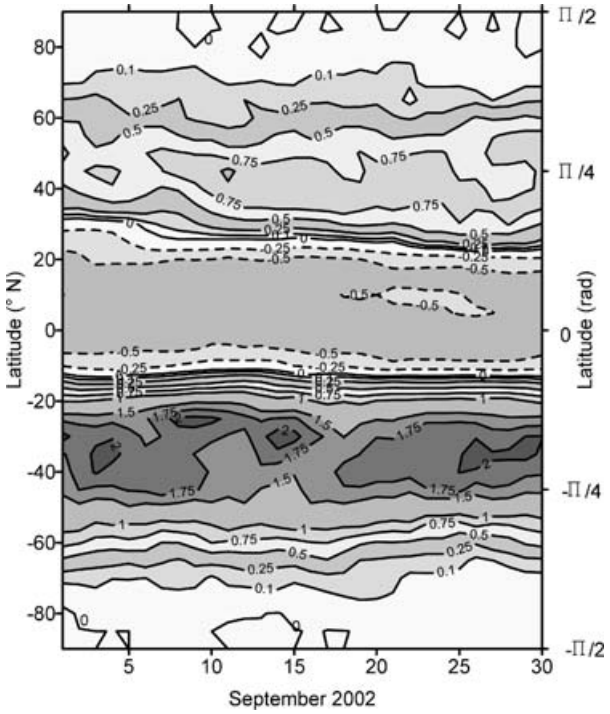

Fig. 3. Relative atmospheric angular momentum, vertically and zonally integrated. The values are normalized with the Earth's radius as factor, which gives units of 10^{26} kg m^2 s^{-1} rad^{-1}. A latitudinal integral over the respective radian interval defines the global and hemispheric AAM shown in Fig. 2. A latitudinal integral over the respective radian interval from the South Pole to a specified but variable latitude defines the AAM of polar caps shown in Fig. 4.

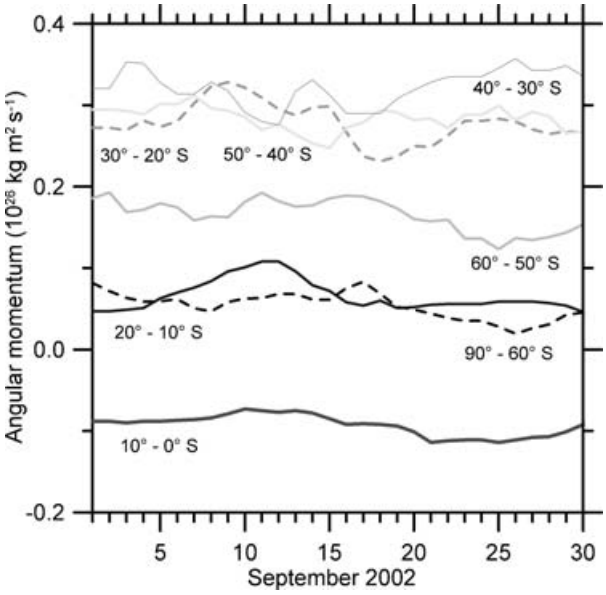

Fig. 4. Evolution of relative atmospheric angular momentum in 10^{26} kg m^2 s^{-1} for southern hemispheric polar cap (90°–60° S, thick dashed line) and latitudinal bands in September 2002.

values of AAM are extending continuously southwards during the month.

For the Southern Hemisphere, a relatively broad maximum of AAM was found between 20° and 50° S at about day 9 as well as a broad minimum between day 16 and 21. This explains the specific evolution of the southern hemispheric curve in Fig. 2 during these days. On average, the mid-latitude increase towards the end of the month is compensated by a decrease of AAM in polar latitudes. This decrease of relative AAM is very important for this investigation because it seems to be related to the polar vortex break-up during the unexpected major warming event in the fourth week of September 2002.

In order to study the austral relative AAM distribution, the mean relative AAM was calculated for a polar cap (90°–60° S) and different latitudinal bands. The results are presented in Fig. 4. The polar cap AAM accounts for less than 10% of southern hemispheric relative AAM of about 1.1 × 10^{26} kg m^2 s^{-1} (Table 1), and is comparable with that of the latitudinal band from 20° to 10° S. The tropical latitudes (10°–0° S) reduce the relative AAM by about 10%. Further, Fig. 4 shows that the maximum of relative AAM at day 9 was mainly generated in the subtropics and tropics (30°–10° S). On average, after day 18 the AAM curves for bands (50°–40° S, 40°–30° S, 30°–20° S) show an increasing or quasi-constant behaviour, but a decrease for the AAM of polar cap and that of the latitudinal band (60°–50° S). This finding supports the result of Fig. 2 that the AAM values of middle and higher latitudes compensate each other during the polar vortex break-up. On average, the relative AAM of polar cap volume southward of 50° S decreases during the month of September 2002. For latitudes from 50° to 20° S, Fig. 4 shows an AAM increase.

One aim of this investigation is to examine the evolution of relative AAM of the polar cap over Antarctica ($\varphi_{PC} = 60°$ S). For different atmospheric layers based on fixed hybrid levels of ECMWF data, the results are plotted in Fig. 5. We found that in the monthly mean about 15% of relative AAM (about 0.08 × 10^{26} kg m^2 s^{-1}) is related to the altitudinal region higher than 32 hPa (about 25 km altitude). About 60 % of AAM belongs to the region between 303 hPa (∼9 km) and 32 hPa (∼25 km) of the stratosphere, and about 25% of relative AAM to the tropospheric region below 303 hPa. The relative AAM of this polar cap atmosphere reached a maximum at day 17 and a minimum at day 26 (see Fig. 4). A relative minimum of AAM was also found at day 8. This relative minimum of AAM of the polar cap (90°–60° S) was built up by the troposphere and lower stratosphere (Fig. 5). The maximum at about day 17 (Fig. 4) shows a barotropic character; with the increase occurring in all layers simultaneously (Fig. 5).

However, the following strong decrease in Fig. 4 was built up in the lower troposphere (Fig. 5). The decrease of AAM after day 20 (Fig. 4) was mainly generated in the stratosphere (Fig. 5)

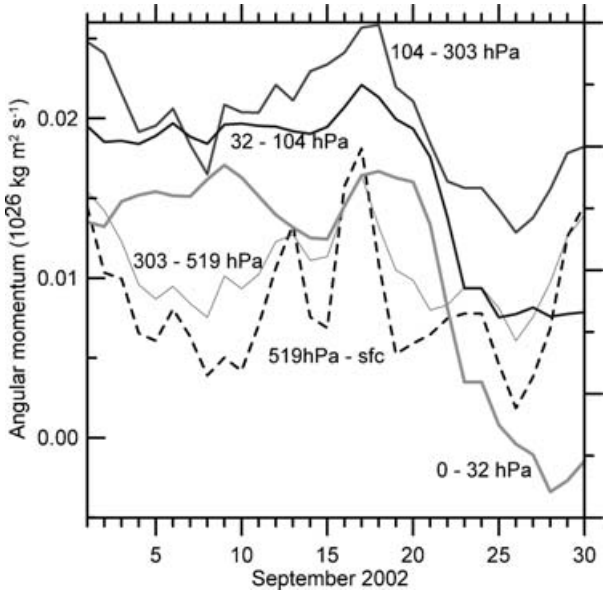

Fig. 5. Evolution of relative atmospheric angular momentum of the polar cap (90°–60° S) in 10^{26} kg m^2 s^{-1} for different layers of the atmosphere.

through the break-up of the polar vortex, and reached negative values in the upper stratosphere caused by the reversal of the zonal mean zonal wind (wind direction from west to east, southward of 60° S). In Fig. 5, the minimum of AAM occurred first in the troposphere (day 26) and 2 d later in the stratosphere. The increase of AAM, after day 26, is mainly determined by the troposphere and lower stratosphere. A comparison with the evolution of the zonally averaged zonal wind (see Fig. 1) will be given in the discussion section.

3.2. *Extra-tropical southern hemispheric AAM tendency and torques*

Following the equation of conservation of angular momentum, eq. (6), the tendency of AAM as a function of southern hemispheric polar cap integrals up to 30° S has been shown in Fig. 6 for absolute, relative and Ω-AAM in order to examine the latitudinal variability in extratropics. The tendency of Ω-AAM is mainly determined by air mass translations due to the Hadley cell, and this process is concentrated in subtropics and tropics of both hemispheres. It follows that in extratropics the tendency of relative AAM of polar cap integrals dominates the absolute AAM. For polar caps extending to between (90°–80° S) and (90°–40° S), this tendency (Fig. 6a) shows a periodic behaviour with an oscillation period of 5 d from the beginning of September 2002 until day 17. Then, a steady decrease occurred until day 26, and afterwards an increase was observed. The agreement between the temporal development of the tendency of relative AAM of the polar cap (90°–60° S) with that of the temporal derivative of the respective curve in Fig. 4 is obvious.

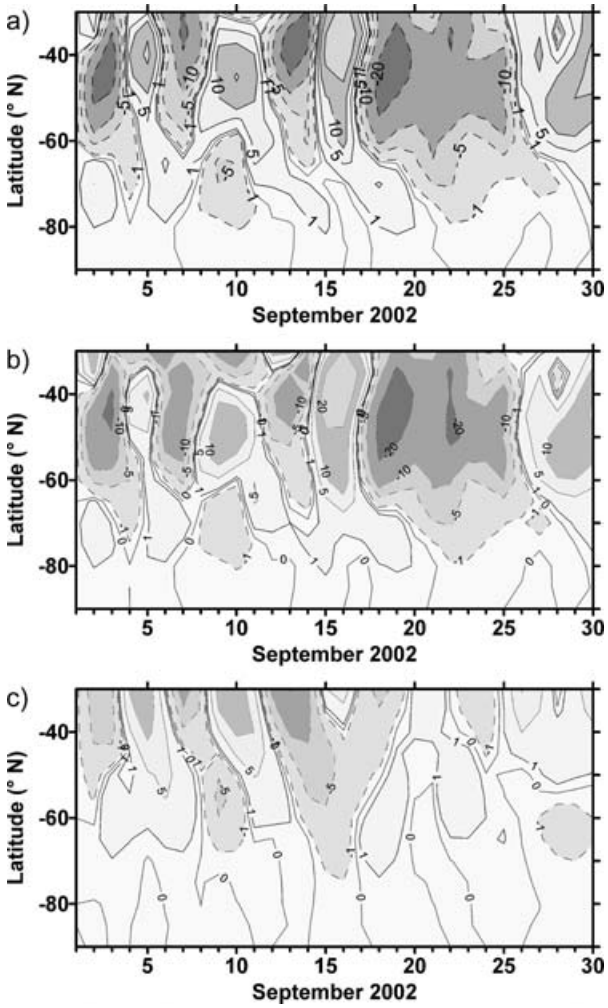

Fig. 6. Atmospheric angular momentum tendency in 10^{18} kg m^2 s^{-2} as function of southern hemispheric polar caps: (a) absolute atmospheric angular momentum tendency, (b) relative and (c) Ω-AAM tendency.

Due to the divergence theorem, the mean negative flux through a virtual wall of specified latitude is equal to the polar cap integral of the convergence of related AAM flux from the South Pole to that specified latitude. The polar cap integral of the convergence of AAM fluxes (or negative AAM flux) is plotted in Fig. 7 for absolute, relative and Ω-AAM as functions of the latitudinal wall and time. In regions northward of 50° S, a growing quasi-periodic absolute AAM flux (Fig. 7a) dominates, which means that there were strong southward and weaker northward-directed AAM fluxes. South of 50° S, there we found strong northward-directed AAM fluxes, which cause the observed convergence in polar latitudes.

The strong convergence of AAM fluxes for polar caps between (90°–70° S) and (90°–50° S) from day 6 to 10 as well as from day 18 to 25 is remarkable. Further, follows from Fig. 7, that the flux of relative AAM (Fig. 7b) dominates that of absolute AAM

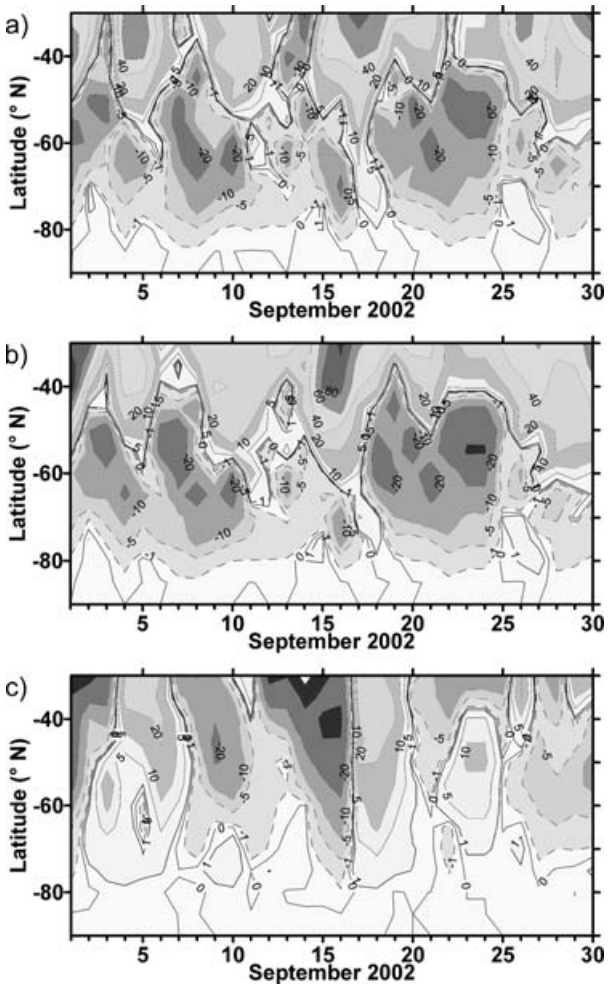

Fig. 7. Negative atmospheric angular momentum flux in 10^{18} kg m^2 s^{-2} for southern hemisphere: (a) absolute angular momentum flux, (b) relative angular momentum flux, (c) Ω-angular momentum flux.

(Fig. 7a) southward of 60° S because the Ω-AAM flux (Fig. 7c) is relatively weak, but it is important in mid-latitudes.

In the monthly mean of September 2002 the northward flux of AAM (see Fig. 7a) goes to zero at about 50° N and changes its sign further northwards, that means we have a southward flux of AAM north of 50° S and a northward flux south of this latitude. This is in agreement with GCM simulations of Peters and Egger (1993) for mean winter flows. In the monthly mean of September 2002, this northward flux of AAM peaks between 60° S and 70° S.

The second and third balance term of the right-hand side of eq. (6), the mountain and the friction torque of polar cap integrals, are plotted in Fig. 8. In addition, in Fig. 9 the mountain and friction torque are shown before their latitudinal integral (eq. (9)) was calculated, but after the longitudinal integration (eq. (8)), as function of radian. The mountain torque of polar cap integrals (Fig. 8a), which are starting at the South Pole show positive

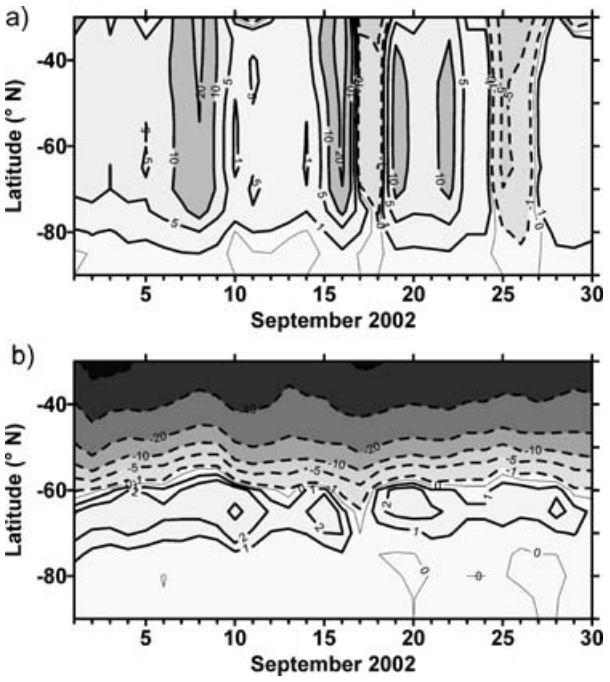

Fig. 8. Atmospheric angular momentum tendency in 10^{18} kg m^2 s^{-2} as function of southern hemispheric polar caps: (a) mountain torque, (b) friction torque.

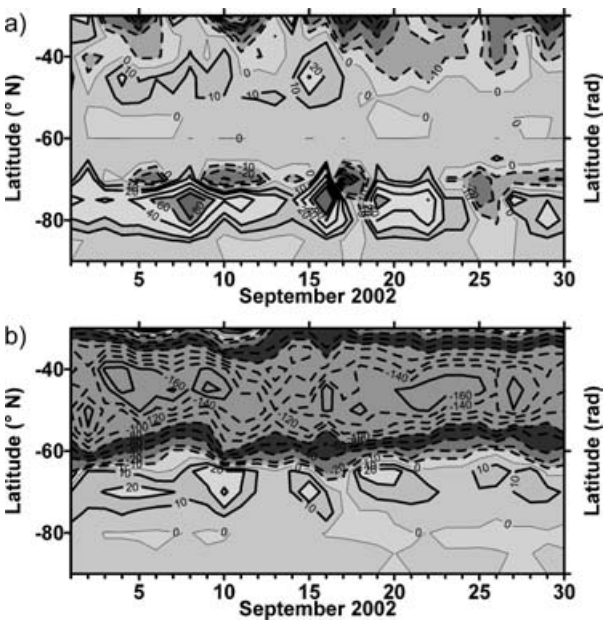

Fig. 9. Atmospheric angular momentum tendency in 10^{18} kg m^2 s^{-2} rad^{-1} as function of southern hemispheric latitudes: (a) mountain torque, (b) friction torque. Both normalized with the Earth's radius as a factor. A latitudinal integral over the respective radian interval from the South Pole to a specified but variable latitude defines the AAM torques of mean polar cap shown in Fig. 10.

values between 70° S and 40° S and relative maxima between day 7 and 9, 15 and 17, 18 and 23. Negative values occurred between day 17 and 18 and from day 24 to 27. Between 70° S and 50° S, the amount of absolute AAM flux (Fig. 7a) and the amount of the mountain torque for polar cap integrals are comparable.

We see from Fig. 9a that the mountain torque is mainly generated in a latitudinal band between 80° S and 65° S and northward of 50° S due to the orography with a strong temporal variability related to surface pressure changes, what explains the high variability found in the integral values of Fig. 8.

For the polar cap integral of friction torque we found a change of sign at about 60° S (Fig. 8b). Up to 60° S, the westward-directed surface winds (katabatic wind of Antarctica, east wind near the coast line) produce a relative small but positive contribution to the AAM balance. Northward of 60° S, the friction torque of polar caps changes its sign, and, northward of 50° S, the amount is distinctly larger than the polar cap mountain torque due to the strong west wind near the surface in mid-latitudes (Fig. 9b). This negative torque is mainly balanced by southward AAM fluxes shown in Fig. 7a.

3.3. AAM tendency and torques over Antarctica

We focus our study on a polar cap volume extended from the South Pole to the coastline of Antarctica, to study the AAM balance during the breakdown of the polar vortex in the September 2002. This was done because the tendency of the relative AAM of such a polar cap over Antarctica is mainly given by the balance between the northward flux of relative AAM (decrease of AAM), the mountain torque (increase of AAM), and friction torque induced by katabatic winds (increase of AAM) as shown before. Two main questions remain: What determines the quasi-periodic behaviour of AAM tendency (about 5 d) until day 18 of September, and what caused the continuous decrease of AAM up to day 27 (with the strongest decrease at about day 23) found in Fig. 6.

We use a mean polar cap volume concentrated around latitude of 65° S, where the mean was calculated from three polar caps (90°–70° S, 90°–65° S, and 90°–60° S) in order to minimize computational errors. A running mean over a 3-d period was applied to exclude high daily variability of AAM results. For such a mean polar cap integral, and to summarize the results, the averaged AAM balance and their components (eq. 6) are presented in Fig. 10. From it follows that the 5-d period of the polar cap AAM tendency before day 18 results from a superposition of anticorrelated oscillations of polar cap integral of the convergence of AAM fluxes and that of mountain torque. Figure 10 confirms that the evolution of the polar cap integral of friction torque is positive and relatively small for polar caps between (90°–70° S) and (90°–60° S) which was already found in Fig. 8b.

The increase of polar cap AAM (positive tendency) between day 4 and 8 was built up by friction torque of the polar cap because the northward flux of AAM and mountain torque of the

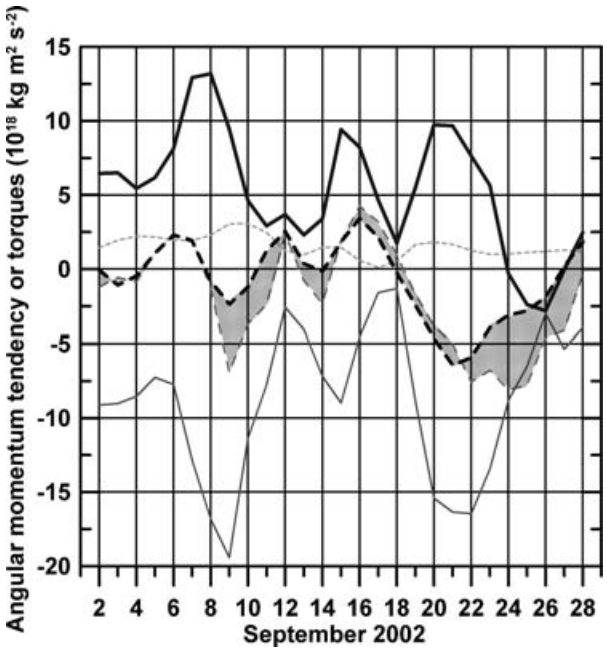

Fig. 10. Mean atmospheric angular momentum tendency of a southern hemispheric polar cap (averaged over three polar caps (90°–70° S, 90°–65° S, 90°–60° S, running mean of 3 d) in 10^{18} kg m^2 s^{-2}, convergence of absolute AAM flux (thin line), mountain torque (thick line), friction torque (short dashed line), sum of all three quantities (thin long dashed line) and AAM tendency (thick long dashed line). Striped area marks the difference between long dashed lines.

polar cap compensate each other. Afterwards, the decrease (day 8–10) is determined by northward flux of relative AAM, and, the increase (day 10–13) again by friction torque of the polar cap. The increase of polar cap AAM (day 14–18) results from mountain torque of the polar cap.

Beginning at day 18, a new evolution of the structure sets in. The polar cap AAM tendency undergoes a longer phase, over 9 d, of negative values decrease with a minimum at about day 22. However, the huge decrease of the northward flux of AAM is not compensated for by increasing mountain torque of the polar cap. Although after day 22 the amounts of both quantities are decaying, the negative tendency through the convergence of AAM fluxes of the polar cap dominates. At day 24, the polar cap mountain torque becomes negative and, additionally, contributes to the decrease of AAM of the polar cap as well as the strongly reduced flux of AAM. In Fig. 10, the sum of all three torques for the polar cap on the right-hand side of eq. (6) is also plotted. The related curve follows mainly that of polar cap AAM tendency and confirms the results shown above. There exists a difference (striped area) between both dashed curves showing the error of calculation. This is discussed further in the next section.

4. Discussion

In order to examine the robustness of the above results, the calculations have been carried out using the ECMWF analysis data

on a $1^\circ \times 1^\circ$ grid, rather than with the spectral components. These calculations produced results very similar to those shown in Figs. 1–10. Further, the calculations were also repeated using 24-hr ECMWF forecast data, with a $3^\circ \times 5^\circ$ grid resolution. The evolution of the AAM and their tendency are also similar to the results presented here (e.g. Fig. 10), except shifted by 1 d, as expected. The difference between AAM tendency and the sum of the right-hand side of eq. (6) was reduced during the vortex break-up. Both additional calculations of the AAM balance show that the results presented are relatively robust. Differences simply indicate the influence of the assimilating model upon the analyses.

The influence of the annual cycle of AAM can also be examined from our analysis. An indication of an annual cycle is the increase of the global mean (Fig. 2), but this global increase of AAM is mainly produced by the increase of AAM in the Northern Hemisphere. The AAM decrease of the Southern Hemisphere during the second part of September 2002 is very weak. So, we assume that the influence of the annual cycle on the results, especially on the strong decrease of polar AAM, to be only minor.

In the following, we discuss the AAM tendency evolution of each component in order to extend our knowledge of the role of different physical processes. We start with the zonal mean friction torque, which is plotted in Fig. 9b. The friction torque is positive in a latitudinal band at about 70° S caused by easterlies. North of this, in mid-latitudes, is a band where relatively strong negative values occur caused by westerlies.

The variability of the positive band at about 70° S is given by the variability of katabatic winds. An example is shown in Fig. 11. The largest friction torque occurred in connection with strong east winds on 10 September (Fig. 11a), but minimum friction torque for weaker east winds on 23 September (Fig. 11b).

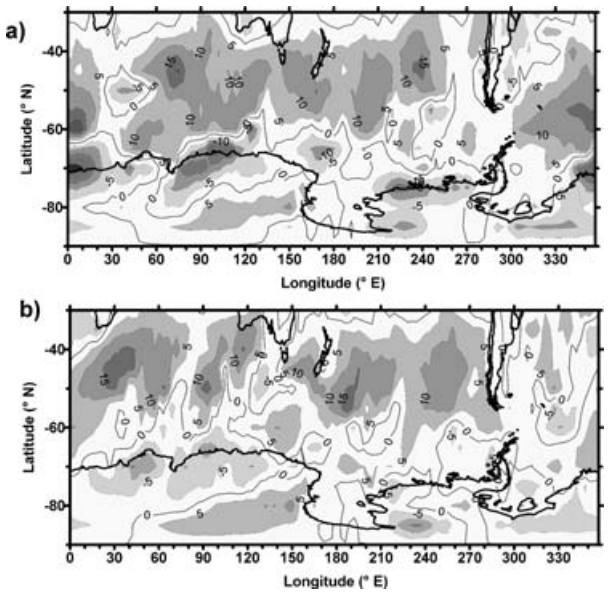

Fig. 11. Zonal wind in m s^{-1} at 10 m height, (a) on 10 September 2002 and (b) on 23 September 2002.

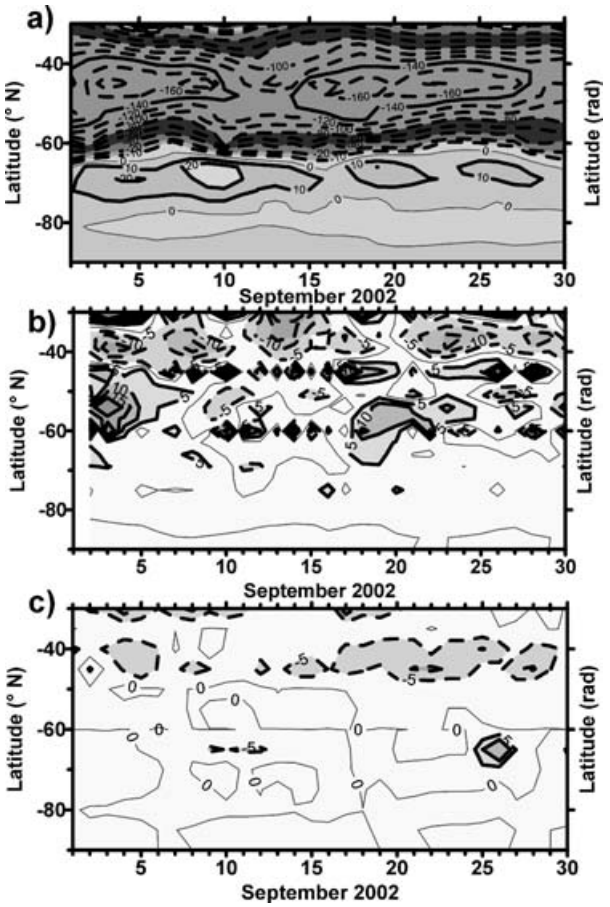

Fig. 12. 24 hr forecasts accumulated torques in 10^{18} kg m^2 s^{-2} rad^{-1}: (a) friction torque and (c) gravity wave drag torque, (b) difference between friction torques (analysis minus forecast).

Friction torque and gravity wave drag torque (due to unresolved orography) are available as accumulated values based on parametrization schemes (White, 2003) used in the 24 hr ECMWF forecast data set. The zonal surface stress components were extracted from MARS archive. The zonal mean of these surface quantities are plotted in Figs. 12a and c by using the integrals defined in eqs. (8) and (9). The difference of friction torques of Figs. 9a minus that of Fig. 12a (but 1 d before) is shown in Fig. 12b. Southwards of 60° S indicate that the bulk formula (10) gives small differences between the ECMWF analyses and forecasts. The variability of positive friction torque values (Fig. 9a) at 70° S agrees quite well with the accumulated forecasts values 1 d before (Fig. 12a). This supports the start we selected for calculating the friction torque.

The gravity wave drag torque has been excluded from our AAM balance. Fig. 12c shows the gravity wave drag torque of the 24-hr ECMWF forecast as described by White (2003). It is

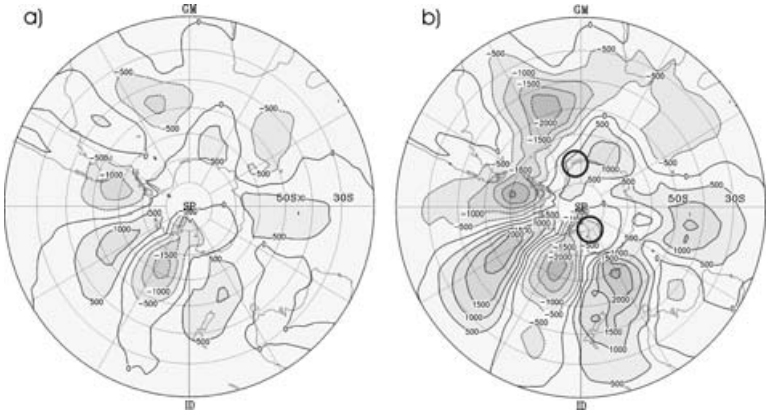

Fig. 13. Stereographic projection of mean surface pressure differences in Pa for different periods of strong and weak mountain torques of polar caps: (a) (25–26) minus (20–21) September 2002, (b) (24–28) minus (18–22) September 2002. A dominant Rossby wave train is starting southeastwards of Australia, crossing the South Pacific, and ending over the South Atlantic. The circles indicate main regions of Eastern Antarctica which are related to the mean mountain torque decrease (about 15×10^{18} kg m^2 s^{-2}) as shown in Fig. 10 during 18–28 September 2002.

relatively small in comparison to the friction torque, and supports our neglecting of this term in earlier calculations of AAM balance. During the polar vortex break-up (25–26 September), a relatively large negative gravity wave drag torque occurred over the edge of Antarctica. Simmons et al. (2003) discussed this fact as a problem of the analysis procedure.

After the polar vortex breakdown a strong reduction of the mountain torque (Figs. 10, 9a and 8a) was observed. This is caused through surface pressure changes about the edge of Antarctica. In Fig. 13, maps of surface pressure difference are shown during that period of strong and weak mountain torques in order to specify the large-scale structure of the flow field.

The shorter period difference map (Fig. 13a, from 20 to 26 September) shows that a Rossby wave train is starting southeastwards of Australia, crossing the South Pacific, propagating over the peninsula of Antarctica, and ending over the South Atlantic. Also in the longer period difference map from day 18 to 28 of September 2002 (Fig. 13b) a similar robust Rossby wave train occurred. This Rossby wave train dominated by waves 1–4 reaches Antarctica and induces an eastward shift of the surface pressure patterns as indicated by the difference maps in Fig. 13.

Based on a spatial Fourier decomposition, we found that in the strong slope regions of Eastern Antarctica the longitudinal decreasing orography correlates with a low-pressure anomaly at about 150° E, and the increasing orography at about GM with a high-pressure anomaly. Through that, the positive mountain torque of polar latitudes decreases and reaches negative values during the major warming phase as shown in Figs. 8a and 10. The negative mountain torque will reduce the AAM. The mean decrease of the polar mountain torque of about 15×10^{18} kg m^2 s^{-2} as shown in Fig. 10 during the period from 18–28 September is mainly related to those pressure surface anomalies as mentioned above. Both main regions are indicated by circles in Fig. 13b.

A similar signal of a Rossby wave train was found in the difference map of geopotential at 300 hPa layer during the same period (not shown) which indicates a Rossby wave train in the free atmosphere.

In a diagnostic investigation, Nishii and Nakamura (2004) also showed the importance of such a Rossby wave train for the major warming during September 2002. They found an enlarged tropospheric forcing region over the Southern Atlantic due to a blocking ridge. The latter was maintained by the Rossby wave train generated over the subtropical western South Pacific some days before the break-up of the vortex. Further, they identified an enhanced tropical convection process as a possible source for Rossby wave generation, and found the same Rossby wave train, as shown in Fig. 13.

Similar Rossby wave trains are observed in multi-year analysis of meteorological quantities of the 500 hPa layer during southern hemispheric spring and summer seasons. There exists also a link to a blocking pattern over the Southeast Pacific (Renwick and Revell, 1999). When investigating the long-term mean in the month September 2002, an abnormal anticyclonic blocking has been observed over West Antarctica (not shown) which could play a similar role. It is known that Rossby wave activity increases over the Southern Hemisphere in austral spring. A possible cause for the forcing of Rossby waves over Australasia could be an excessive tropical heat source as implicated by studies of Karoly et al. (1989), Jin and Hoskins (1995), and Renwick and Revell (1999). That was shown explicitly by Nishii and Nakamura (2004) to happen in September 2002.

Rossby wave propagation over the South Pacific is connected with zonal mean angular momentum transport in the upper troposphere and lower stratosphere. The zonal mean meridional momentum transport is given in Fig. 14 for (a, b) 20–25 and (c, d) 25–30 September. In (a) and (c) the quasi-stationary components are plotted, whereas the transient components are shown in (b) and (d). In the phase of strong AAM fluxes out of the polar cap the quasi-stationary (based on a 5-d mean) as well as the transient waves (deviation from 5-d mean) transport nearly the same amount of momentum out of the polar cap. In polar latitudes the quasi-stationary fluxes are directed northwards in the troposphere and in the stratosphere. In the phase of reduced AAM fluxes (after the polar vortex breakdown), the momentum flux (Fig. 14c, d) induced by Rossby waves is also strongly

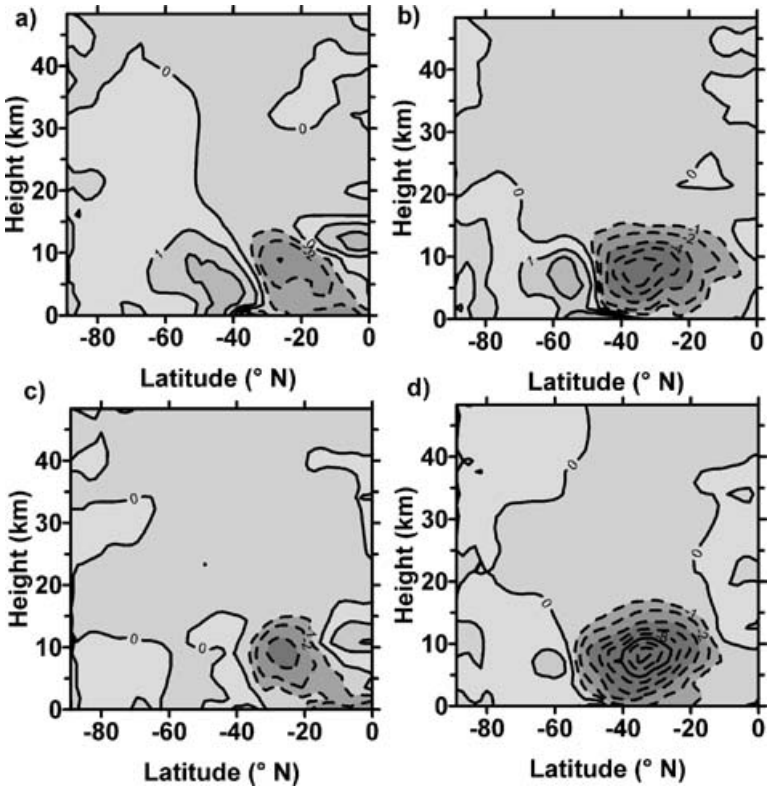

Fig. 14. Meridional transport of momentum in $m^2\ s^{-2}$ normalized by $(p/p_s * \cos^2\phi)$ for (a, c) stationary and (b, d) transient waves during period: (a, b) 20–25 September 2002 and (c, d) 25–30 September 2002. Contour interval is 2 $m^2\ s^{-2}$, but 1 $m^2\ s^{-2}$ between $-2\ m^2\ s^{-2}$ and 2 $m^2\ s^{-2}$.

reduced in south polar latitudes. The decrease of AAM in the polar cap starts at day 18, which is in agreement with the Hovmöller diagram of the zonal mean zonal wind at 60° S (Fig. 1), which shows a relative maximum in the stratosphere at just about this day. The minimum of AAM appeared in the troposphere at day 26 and 2 d later in the upper stratosphere (Fig. 5). During this time, the zonal mean zonal wind changed into a very strong east wind by the action of the convergence of Eliassen-Palm fluxes due to tropospheric Rossby waves propagating into the upper stratosphere. From Matsuno's (1971) theory, if strong transient tropospheric Rossby waves propagate upward and cause EP-flux convergences in the upper stratosphere, the zonal mean zonal wind is decelerated suddenly and the air is rapidly warmed adiabatically, by the induced residual descent circulation of the upper polar stratosphere. Both features, which were very intense, have been observed for the first time over the Southern Hemisphere in September 2002 as mentioned in the Introduction. Such events belong to the Berlin phenomenon discovered by Scherhag (1952) over the Northern Hemisphere.

5. Conclusion

In September 2002, the global relative atmospheric angular momentum increased because the boreal AAM increased due to a continuous broadening of the westerlies in mid-latitudes. The austral relative AAM showed a distinct maximum around September 9, which was related to subtropical and tropical processes. After September 20 the relative AAM was nearly constant, as the result of an increase of relative AAM in mid-latitudes and compensated decrease in polar latitudes. For Antarctic polar caps, a relative minimum of relative AAM occurred around September 8, the relative AAM then increased until day 17, and then decreased until day 26. The increase was barotropic but the decrease was larger in the stratosphere. The minimum of relative AAM appeared at first in the troposphere and 2 d later in the stratosphere. The increase after day 26 was mainly determined by tropospheric and lower stratospheric processes.

The evolution of the polar cap AAM tendency shows the dominant role of the change of relative AAM in middle and polar latitudes. It shows a quasi-periodic behaviour between day 1 and 18 and afterwards a relative long interval of AAM decrease. This decrease is linked to the strong convergence of AAM fluxes, due to a strong northward-directed AAM fluxes in polar latitudes. At these latitudes, the absolute AAM flux is determined by relative AAM fluxes especially during the AAM decrease from day 18 to 27. The polar cap mountain torque is highly variable and partially in opposite phase to the convergence of AAM fluxes. The friction torque induced by katabatic winds is positive, relatively small, and weakly variable in austral polar latitudes.

The analysis of the polar cap AAM balance showed that the mountain and the friction torque are permanently positive and represent a source of AAM with the exception of the mountain torque after day 24. The convergence of AAM fluxes acts as a sink of AAM and is anticorrelated to the mountain torque. Both are

highly variable. The sum of all three quantities defines the AAM tendency with an oscillation of a 5-d period from the beginning till day 18 of September. Afterwards, a relatively long interval of AAM decrease (day 18–27) results from a negative balance between the generation of AAM by mountain torque (friction torque is small) and the loss of AAM by northward transport of AAM out of the polar cap. The mountain (and friction) torque do not compensate the export of AAM out of the polar cap over Antarctica, so that an abnormal long interval of AAM decrease in polar latitudes occurred which was concentrated in the stratosphere, and which caused a wind reversal above 10 hPa during the polar vortex break-up and the related warming. The relatively long and strong AAM decrease starting at day 18 was related to an intensive Rossby wave train, which extended from Australia, over the peninsula of Antarctica to the Southern Atlantic touching the edge of Antarctica. An extensive forcing over the western South Pacific through enhanced tropical convection generates the eastward travelling Rossby wave (Nishii and Nakamura, 2004).

An extension of this AAM analysis to polar caps of the Southern and Northern Hemisphere would enable an investigation of the seasonal, annual, interannual or decadal changes of AAM, their tendency, and the importance of their components for the AAM balance. The balance between the convergence of AAM fluxes, mountain torque and friction torque of polar caps is a good indicator of generation or loss of AAM due to changes of the general circulation.

6. Acknowledgements

The authors thank the Deutscher Wetterdienst and ECMWF in Reading for providing the ECMWF analyses and 24-hr-forecast data set. We gratefully acknowledge the help of Frau H. Voss in calculating momentum fluxes. We thank G. Schmitz, E. Hagen and R. Feistel for fruitful discussions; J. Alheit, D. Waugh and two anonymous reviewers for improving of the manuscript.

References

Baldwin, M., Hirooka, T., O'Neill, A. and Yoden, S. 2003. Major stratospheric warming in the southern hemisphere in 2002: dynamical aspects of the ozone hole split. *SPARC newsletter no.* **20**, 24–26.

Egger, J. 1992. Topographic wave modification and the angular momentum balance of the Antarctic troposphere. *J. Atmos. Sci.* **49**, 327–334.

Egger, J. and Hoinka, K.-P. 2002. Covariance analysis of the global atmospheric axial angular momentum budget. *Mon. Wea. Rev.* **130**, 1063–1070.

Iskenderian, H. and Salstein, D. A. 1998. Regional sources of mountain torque variability and high-frequency fluctuations in atmospheric angular momentum. *Mon. Wea. Rev.* **126**, 1681–1694.

Jin, F. and Hoskins, B. J. 1995. The direct response to tropical heating in a baroclinic atmosphere. *J. Atmos. Sci.* **52**, 307–319.

Karoly, D. J., Plumb, R. A. and Ting, M. 1989. Examples of the horizontal propagation of quasi-stationary waves. *J. Atmos. Sci.* **46**, 2802–2811.

Krueger, K., Naujokat, B. and Labitzke, K. 2005. The unusual midwinter warming in the Southern Hemisphere Stratosphere 2002: a comparison to Northern Hemisphere phenomena. *J. Atmos. Sci.* **62**, 603–613.

Madden, R. A. and Speth, P. 1995. Estimates of atmospheric angular momentum, friction, and mountain torque during 1987–1988. *J. Atmos. Sci.* **52**, 3681–3694.

Matsuno, T. 1971. A dynamical model of stratospheric sudden warming. *J. Atmos. Sci.* **28**, 1479–1494.

Newton, C. W. 1971. Mountain torques in the global angular momentum balance. *J. Atmos. Sci.* **28**, 623–628.

Nishii, K. and Nakamura, H. 2004. Tropospheric influence on the diminished Antarctic ozone hole in September 2002. *Geophys. Res. Lett.* **31**, doi:10.1029/2004GL019532.

Peixoto, J. and Oort, A. 1992. *Physics of climate*. American Institute of Physics, New York, 624p.

Peters, D. and Egger, J. 1993. Antarctic slope winds without surface cooling: experiments with a general circulation model. *Contrib. Atmos. Phys.* **66**, 253–258.

Renwick, J. A. and Revell, M. J. 1999. Blocking over the South Pacific and Rossby wave propagation. *Mon. Wea. Rev.* **127**, 2233–2247.

Rosen, R. D., Salstein, D. A., Miller, A. and Arpe, K. 1987. Accuracy of atmospheric angular momentum estimates from operational analyses. *Mon. Wea. Rev.* **115**, 1627–1639.

Salby, M. L. 1996. *Fundamentals of atmospheric physics*. Academic Press, San Diego, 627p.

Scherhag, R. 1952. Die explosionsartigen Stratosphärenerwärmungen des Spätwinters 1951/52. *Berichte des Deutschen Wetterdienstes in der US-Zone* **6, Nr. 38**, 51–63.

Schwerdtfeger, W. 1984. *Weather and Climate of the Antarctic*. Developments in atmospheric science **15**. Elsevier, Amsterdam, 261p.

Simmons, A., Hortal, M., Kelly, G., McNally, A., Untch, A., and coauthors. 2003. Analyses and forecasts of stratospheric winter polar vortex break-up: September 2002 in the southern hemisphere and related events from ECMWF operations and ERA-40. ERA-40 project report series no. *5*, The Library ECMWF, Reading, 28p.

Weickmann, K. M. 2003. Mountains, the global friction torque, and the circulation over the pacific-North American Region. *Mon. Wea. Rev.* **131**, 2608–2622.

Weickmann, K. M., Robinson, W. A. and Penland, C. 2000. Stochastic and oscillatory forcing of global atmospheric angular momentum. *J. Geophys. Res.* **105**, 15 543–15 557.

White, P. W., 2003. IFS Documentation, Part IV: Physical processes (CY25r1). The Library ECMWF, Reading, 164 p., see section 3.8.2.